http://www.jmaterenvironsci.com/

Effect of abrasive particles on electrochemical behaviour of passive film formed on Alloy 59 in contaminated phosphoric acid

S. Skal[1]*, Y. Kerroum[1], A. Guenbour[1], A. Bellaouchou[1], H. Tabyaoui[1], H. Idrissi[2], A. Zarrouk[3] and J. García-Antón[4]

1. Laboratoire des Matériaux Nanotechnologie et Environnement, Université Mohamed V Agdal. Faculté des Sciences. Av. Ibn Battouta. BP 1014, Rabat. Maroc
2. MATEIS Bât. B. Pascal, 5° étage - 7, avenue Jean Capelle –INSA, 69621 Villeurbanne cedex –France
3. LC2AME, Faculty of Science, First Mohammed University, PO Box 717, 60 000 Oujda, Morocco
4. Ingeniería Electroquímica y Corrosión (IEC), Departamento de Ingeniería Química y Nuclear, ETSI Industriales, Universitat Politècnica de Valencia, P.O. Box 22012, 46071 Valencia, Spain

Abstract

The effect of abrasive on electrochemical behaviour of passive film formed on a austenitic stainless steel alloy 59 (UNS N-06059) in polluted phosphoric acid without and with abrasive grit was investigated by potentiodynamic and potentiostatic electrochemical measurements, electrochemical impedance spectroscopy and Mott-Schottky analysis. The results indicated that this alloy exhibited well passive behaviour with and without abrasive. In polluted phosphoric acid, the abrasion causes an electrochemical process acceleration leading to a decrease in the resistance and an increase in the capacity of material. The film formed on steel surface was of p-type and n-type semiconductors in the potential range below and above the flat band potential, respectively. The alloy 59 shows good resistance in the abrasion-corrosion according to his high chromium content, 22.65% Cr provided by the inner oxide film, while the outer film was more defective.

1. Introduction

The phenomenon of corrosion-abrasion is responsible for the premature destruction of numerous industrial installations in which corrosive fluids circulate, together with another phase, essentially a solid one [1]. In addition to the deterioration resulting from electrochemical corrosion, a mechanical damage results from the velocity of the fluid and particularly from the interactions between the particles in suspension and the surface of the impacted material [2]. The complexity of the phenomenon is due to the effects of various interactions between the hydrodynamic, mechanical and electrochemical degradation processes, which involve a great number of parameters such as:

➤ parameters linked to the environment: pH, composition, temperature and viscosity of the fluid and characteristics of the particles in suspension (size, morphology, hardness, concentration…);
➤ parameters linked to the material: composition, hardness, structure and morphology of the surface (inclusions, roughness, state of passivation, …);
➤ parameters related to the impingement conditions: angle of impact, flow rate of the fluid and nature of the flow.

In industrial environment, many materials are subjected to the abrasion-corrosion phenomenon. In such cases, stainless steels are often used for their good corrosion resistance. However, the synergistic effect between abrasion and corrosion may be a serious contributor to the total wear even when pure corrosion rates do not appear to be significant.

In the wet production industry, phosphoric acid is obtained from natural phosphates by acid attack, usually sulfuric acid [3]. The acid produced contains various impurities, including aggressive agents such as chloride,

fluoride, sulphate, and sulfide , increase the risk of damage to corrosion depending on the type of stainless steel used, the metal cations have an inhibitory effect and solid particles of gypsum in suspension relative to the abrasion-corrosion.

It has been show that abrasion-corrosion causes an acceleration electrochemical process leading to a decrease in the resistance of materials [4]. Precisely, the synergistic effect between the chemical impurities and the abrasive having consequent increases the corrosion rate. It has been demonstrated by using different approaches [5,6]. The resistance of abrasion-corrosion is directly related to the passivating element content in the alloy (Cr-Mo) such as Alloy 31 [7-9] and Alloy 22 [10-12].

It is known that Alloy 59 has the highest chromium (22.65%) and molybdenum (15.40%) content with the lowest iron content of typically less than 1%. Due to its excellent corrosion resistance, several interesting studies have been reported on the corrosion behaviour in the hydrofluoric acid production, coal-fired power plants, sulfuric acid and sodium thiosulfate solutions [13-15].

In our laboratory, several works studied the corrosion of diverse materials in the phosphoric acid and in the hydrochloric acid with addition of a different inhibitor [16-19] and sometimes measurements were performed in the industrial phosphoric acid with addition of solid particles to study the abrasion effect realized by Guenbour et al. [20]. However, there are limited studies on the electrochemical and passive behaviour of the alloy 59 in the polluted phosphoric acid with abrasive.

The aim of the present work is to propose a study of the abrasion-corrosion behavior, the electrochemical and the electronic properties of passive films formed on the austenitic stainless steel alloy 59 (UNS N-06059) used in the phosphoric industry where the highly concentrated phosphoric acid medium (40%) polluted with sulphate and chloride ions is produced. This study was carried by potentiodynamic and potentiostatic electrochemical measurements, electrochemical impedance spectroscopy, Mott-Schottky analysis and by ex-situ surface analytical technique as optical microscope.

2. Materials and methods

2.1. Materials

The stainless steel used in this study is a highly alloyed steel (UNS N-06059). Its chemical composition is given in Table 1 and its commercial name that will be used all over this work is alloy 59. Each of these components has a positive property of the corrosion resistance. In fact, the percentage of Ni increases the corrosion resistance by increasing the critical potential, the percentage of Cr results in a high resistance to corrosion due to the protective oxide layer formed on the surface. Finally the percentage of Mo improves the corrosion resistance and facilities the passivation after the rupture of the passive film [21-23].

The cylindrical electrodes used were welded to a copper wire for the electrical contact and embedded in an epoxy resin so as to avoid crevice corrosion and leaving only an active area of 0.5 cm^2 in contact with the electrolyte.

Prior to immersion in the electrochemical cell, electrodes were wet-ground with a series of SiC paper of decreasing grit size (180-1500), followed by rinsing with distilled water and dried within a stream of air.

Table 1: Chemical composition of alloy 59 austenitic stainless steel (wt.%).

Elements	Ni	Cr	Mo	Fe	Mn	C	P	S	Si	Co	Al
wt.%	60.58	22.65	15.40	0.58	0.15	0.002	0.003	0.002	0.03	0.04	0.16

2.2. Montage

The arrangement used for the present abrasion studies is illustrated in Figure 1. It formed by a cell (a) with a lateral opening for the introduction of a nozzle (b) and working electrode (d). This later allows us to study the effect of the projection angle (90°) of the aggressive solution. This cell cover has orifices allowing the insertion of a platinum counter electrode (f) and a saturated calomel reference electrode (e). In addition, a peristaltic pump (c) with variable speed controlled the injection rate of the abrasive electrolyte.

2.3. Solution and electrochemical measurements

The samples were tested in a polluted 40 wt.% phosphoric acid solution with addition 4 wt.% of H_2SO_4 and 0.42 wt.% KCl, typical concentrations for the phosphoric acid industry, with and without abrasive.

The abrasive selected is a silicon carbide (SiC). These chemically inert particles have forms enough acutes causing efficient abrasion and reproducible in our laboratory [24] showed in the following Figure 2:
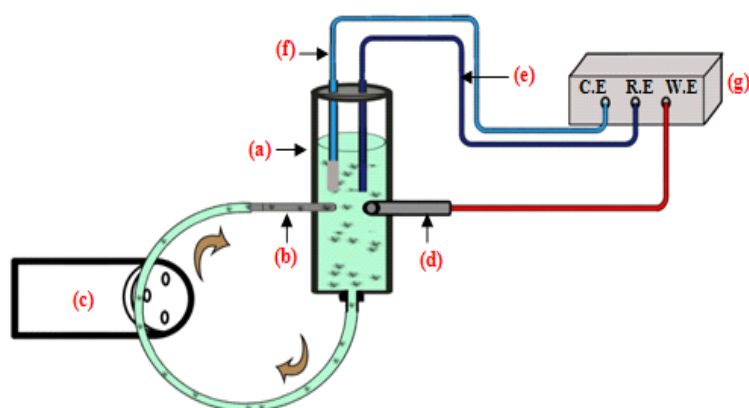
Figure 1: An abrasion-corrosion test: **(a)** Cell **(b)** Nozzle **(c)** Peristaltic pump **(d)** W.E **(e)** R.E (SCE) **(f)** C.E (Pt) et **(g)** Potentiostat.

Figure 2: Morphology of the SiC particles using in abrasion-corrosion

Electrochemical measurements were performed by using a Voltalab PGZ 301 potentiostat. Prior to the measurements, the working electrodes were initially reduced potentiostatically at - 600 mV / SCE for 60 s to remove air-formed oxides

2.3.1. Potentiodynamic tests

The potentiodynamic curves were recorded potentiodynamically using a scan rate of 1 mV s^{-1} starting from - 0.160 V vs. OCP (Open Circuit Potential) with abrasive and starting from - 0.080 V vs.OCP without abrasive. These tests were used not only to give information about general electrochemical behaviour but also to determine the following electrochemical parameters; corrosion current density (i_{corr}), corrosion potential (E_{corr}) and the transpassive potential (E_{tr}) which is defined as the potential where the current density reaches 100 $\mu A/cm^2$. The current density before E_{tr} is almost constant during a range of potentials where the passive current density (i_p) can be estimated as an average of this range.

2.3.2. Potentiostatic tests

The potentiostatic passivation tests were performed in order to obtain the current transient at a constant applied potential. The imposed potential of 600 mV/SCE was selected according to the potentiodynamic curves, since this potential lies within the passive range. Then the chosen potential was applied for 2 h and the potentiostatic current density transients were recorded.

2.3.3. Impedance and capacitance tests

EIS and capacitance measurements were performed after potentiostatic passivation tests, once a stable passive film was formed on the samples surface. The electrochemical impedance spectroscopy (EIS) was conducted in

the frequency range of 100 kHz -100 mHz, with amplitude signal of 10 mV peak to peak. The impedance diagrams are given in the Nyquist and Bode representations. The impedance data were analysed and fitted with the simulation ZView 2.80, equivalent circuit software. Subsequently, the capacitance measurements were performed on the films at a fixed frequency of 5 kHz during a 25 mV/Step in the potential range from -0.6 to 0.6 V (vs. SCE). It ensures that the defect concentrations and the film thickness remain 'frozen' at the formation values while the capacitance is being measured as a function of potential.

2.3.4.Microscopic observations

The optical microscopy observations of metal surface (micrograph) were performed with an optical microscope Leica CTR 6000 (Optical microscope type DFC 295) allowing for magnifications of 50 to 1000 times. A digital sensor mounted on the microscope used to view the different microstructures of our parts. Both surfaces (with and without abrasive) were observed with this equipment.

3. Results and discussion

3.1 Potentiodynamic polarization behavior

Figure 4 shows the potentiodynamic polarisation plots of Alloy 59 in the contaminated phosphoric acid solution with and without abrasive. Alloy 59 displays similar polarization curves for both tests, showing a very wide potential domain of passivity, generally in the potential range between 0.239 V/SCE and 1 V/SCE without abrasive and between 0.186 V/SCE and 1 V/SCE with abrasive particles. Thus, these have been the selected potential range to study the properties of the passive film formed on Alloy 59. In addition, From the 1 V/SCE potential, the sharp increase in current density for both tests indicates the breakdown of the passive film, showing the trans-passive region of Alloy 59 in the phosphoric acid solution without and with abrasive.

In addition, it is noted that the trans-passive potential E_{tr}, at which the breakdown of the passive film happened, shifted towards more active values as the added particles situation.
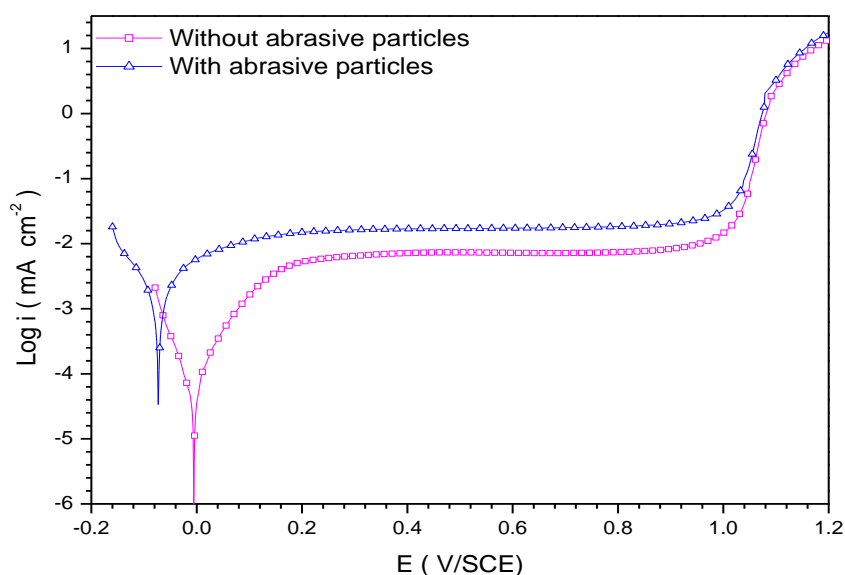

Figure 4: Potentiodynamic polarization curves of Alloy 59 in contaminated phosphoric acid solution (a) without and (b) with abrasive particles.

In fact, this behavior is attributed to the chemical composition of the studied alloy rich on Cr and Ni. At anodic potentials, the formation of Ni and Cr oxides was expected according to these reactions:

$$Ni + H_2O \longleftrightarrow NiO + 2H^+ + 2e^-$$
$$Cr + H_2O \longleftrightarrow CrO + 2H^+ + 2e^-$$
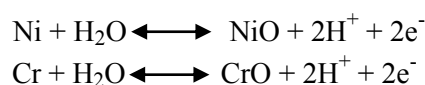
Whereas, the formation of both chrominum and nickel oxides took place by direct nucleation and growth mechanism on the electrode surface. Then, the formation of higher oxidized form of chromium was expected as well as some thickenin of nickel oxide [25],

$$2CrO + H_2O \longleftrightarrow Cr_2O_3 + 2H^+ + 2e^-.$$

However, the corrosion potentials (E_{corr}), corrosion current densities (i_{corr}), passive current densities (i_p) and transpassive potentials (E_{tr}) were obtained from the potentiodynamic polarization curves. The corresponding numerical values are summarized in Table 2.

Table 2: Electrochemical parameters of Alloy 59 in the contaminated phosphoric acid solution without and with abrasive particles

Parameters	without abrasive particles	with abrasive particles (24 g L^{-1} of SiC)
E_{corr} (mV/SCE)	-5.5	-73
E_{tr} (mV/SCE)	884	821
i_{corr} (μA cm^{-2})	3.6	8.6
i_{pas} (μA cm^{-2})	7.22	17.32

It is observed from this Table, that the added particles induce a shift in the corrosion potentials (E_{corr}) towards more negative value, from -5.5 mV/SCE to -73 mV/SCE with an increase in the corrosion current density (i_{corr}) and passive current density (i_p) values, from 3.6 μA cm^{-2} to 8.6 μA cm^{-2} and 7.22 μA cm^{-2} to 17.32 μA cm^{-2}, respectively. The increase of E_{corr} and i_{corr} seems to be related to the enhancement of the cathodic reaction with the presence of abrasive particles. In addition, the increase of i_{pas} can be associated with the growth of the passive film which is enhanced by adding the abrasive [26-28]. The same effect was observed by Escrivà-Cerdán et al. when they studied the effect of potential formation on the electrochemical behaviour of a highly alloyed austenitic stainless steel in contaminated phosphoric acid at different temperatures [29].

However, the trans-passive potential, E_{tr}, decreased slightly with presence of abrasive particles, due to the anodic dissolution of the Alloy 59 leading to a loss of its passivity. In general, the effect of particles in the solution is more significant due to the presence of aggressive ions affecting the anodic branch [30]. This result reveals that the passive films formed in the absence of abrasive particles significantly less defective and more resistant to film break-down than those formed in the presence of abrasive particles.

These results were confirmed by the observation of the surface state using an optical microscope, illustrated in Figure 5. It is observed that the surface of alloy 59 became more rigorous by the presence of the abrasive particles (Figure 5b).
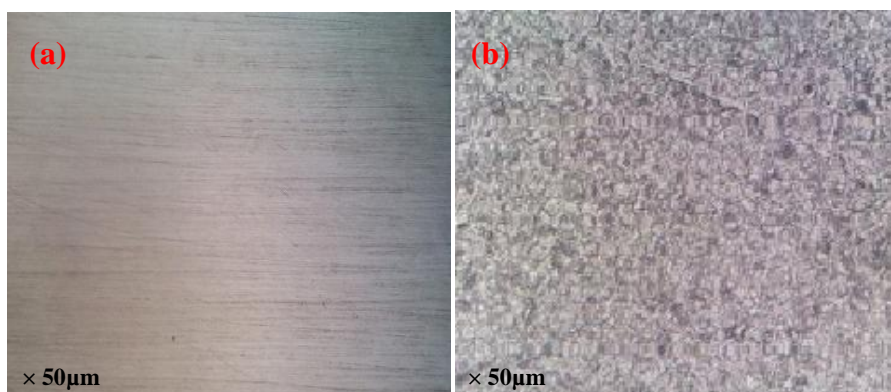

Figure 5: Micrographics of the surface state by an optical microscope of Alloy 59 (a) without and (b) with abrasive particles (abrasion-corrosion)

3.2. Potentiostatic tests

The current–time transients of Alloy 59 obtained at 0.6 V/SCE in the contaminated phosphoric acid solution without and with the presence of abrasive particles are shown in Figure 6. The values of current density recorded during the potentiostatic tests give the total current resulting from the film formation (i_f) and the dissolution (i_D) of Alloy 59 in the solution studied ($i = i_D + i_f$) [31]. It is seen that the shape of the curves is the same without and with the presence of abrasive particles. This suggests that the abrasion does not change the sensitive electrochemical processes at the interface level and the kinetics growth passivity film is apparently the same type [32].

It is noted also that the current density decreases rapidly with time for both cases. This is attributed to the nucleation and growth of the passive film at a rate higher than that of metal dissolution. All current–time transients show that further increase in time resulted in a relatively steady state current density (i_{ss}), indicating the formation of a passive film on the surface of Alloy 59. This i_{ss} is observed to increase with the presence of abrasive particles (Table 3), indicating a reduction in the protective nature of the passive film.

The time–current density relationship can be expressed by the following empirical equation [33]:

$$i = At^{-n} \tag{1}$$

where i denotes the anodic current density consumed in the building of the passive film, A is a constant, t is the time, and n is the passivation index, which is a constant value for a given environment-metal system. This parameter can be obtained from the fitting used Origin Software and it has been considered as an indirect measure of the rate of formation of the passive film upon the fresh metal surface, being primarily dependent upon the applied anodic potential [34,35]. According to the literature [36,37], when n = 1 indicates the formation of a compact, highly protective passive film, while n = 0.5 indicates the presence of a porous film growing as a result of a dissolution and precipitation process.

Table 3 summarizes the values of n for Alloy 59. The high decrease of this parameter with the presence of abrasive particles is an indication that the protective properties of the passive films decrease with the presence of these particles and confirmed the obtained results by optical microscope.
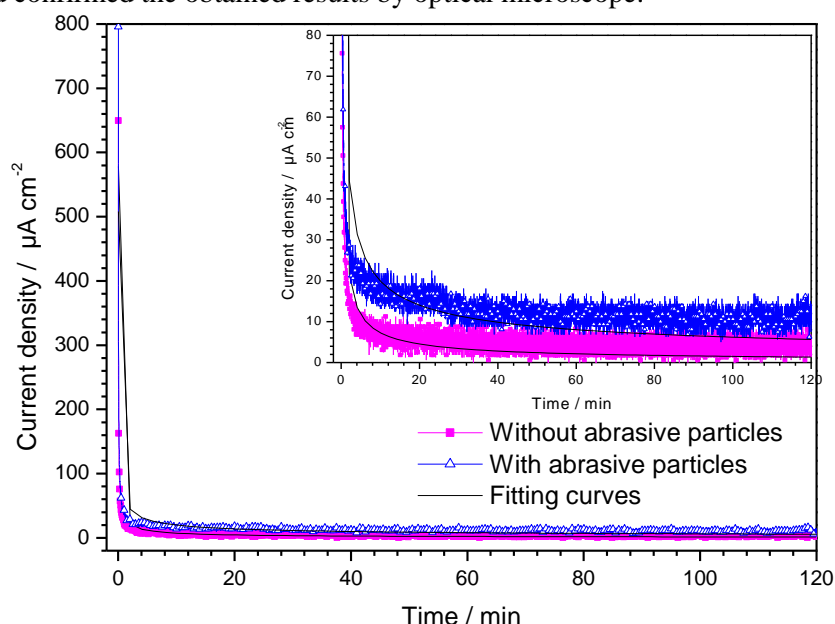

Figure 6: Current–time transients plots of current time for Alloy 59 after 2 h of immersion in the contaminated phosphoric acid solution without and with abrasive particles.

Table 3: Stable state current density i_{ss} and passivation parameter n for Alloy 59 in the contaminated phosphoric acid solution without and with abrasive particles after 2 h of stabilization of passive films at 0.6 V/SCE.

Parameters	Without abrasive particles	With abrasive particles (24 g L^{-1} of SiC)
i_{ss} ($\mu A\ cm^{-2}$)	3.13	14.38
n	0.6839±0.001	0.5064±0.001

3.3. Impedance spectroscopy tests :

The electrochemical properties of the film formed on the surface of the austenitic stainless steel alloy 59 (UNS N-06059) were measured using impedance spectroscopy (EIS) in the polluted phosphoric acid solution. EIS as a technique has proved capable of accessing relaxation phenomena whose relaxation time varies over orders of magnitude and permits single averaging within an experiment to obtain high precision levels. Thereby, it is nowadays widely applied for investigating the corrosion and passivation phenomena due to its non-destructive nature suitable for corrosion monitoring [38,39]. The impedance responses are presented in Nyquist (Figure 7A) and Bode-phase (Figure 7B).

All impedance spectra present a somewhat unfinished capacitive arc as evidenced from Figure 7A, which show that the overall impedance values slightly decrease in the polluted phosphoric acid with abrasive. This translates into a decrease in the resistance polarization or of transfer, showing an increase in the dissolution of the material. In Figure 7B, the Bode diagram clearly shows that the austenitic stainless steel (Alloy 59) in polluted phosphoric acid solution presents three distinct regions. At high frequencies, it exhibits phase angle values close to $0°$ and $|Z|$ values in the range 1-10 Ω cm^2, indicating that the impedance is dominated by electrolyte resistance. At intermediate frequencies, the values of phase angles reach their maximum and a linear slope was observed, showing a capacitive behaviour and formation of a stable passive film in polluted phosphoric acid without and with abrasive particles. At low frequencies, $|Z|$ values are in the range 10^4-10^5 Ω cm^2.
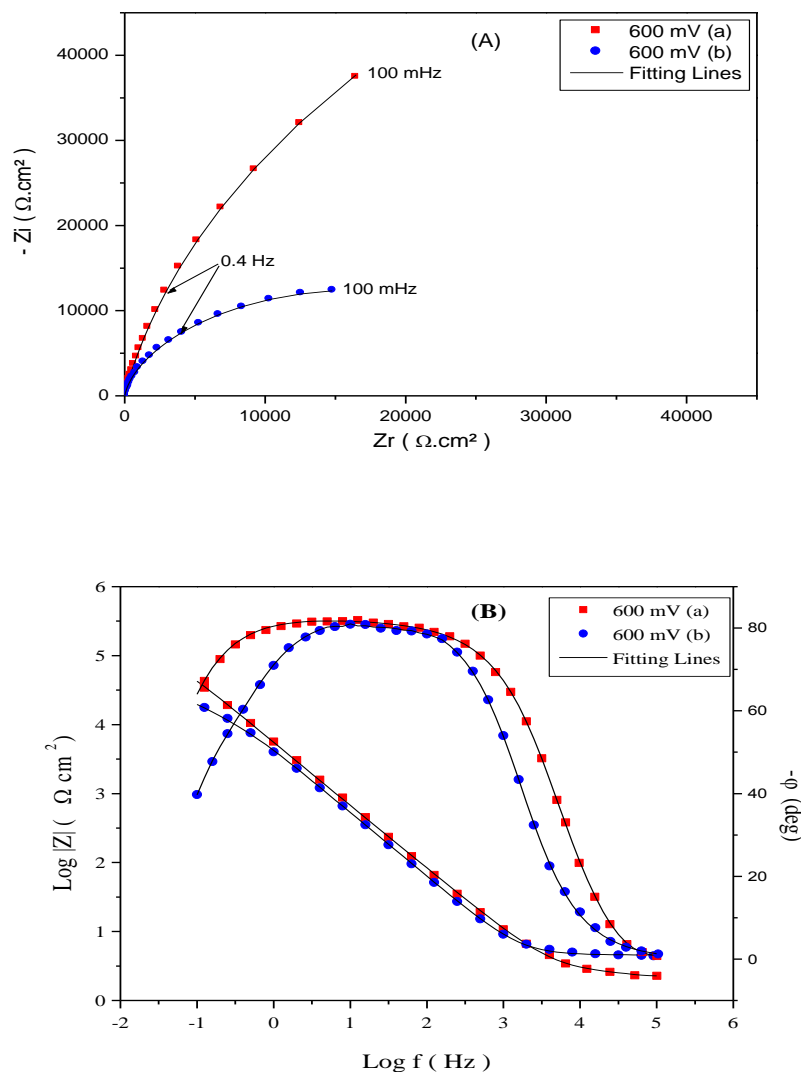

Figure 7: Nyquist diagrams (A) and Bode plots (B) of Alloy 59 after 2 h in polluted phosphoric acid without (a) and with abrasive particles (b) obtained at 600 mV/SCE.

The EIS technique enables us to match the electrochemical system with model circuits consisting of discrete components equivalent to the different parameters of the electrochemical system [40]. From literature, different models have been put forward through the analysis of the EIS of metal/passive film/solution system. Four commonly used electrical equivalent circuits (EEC) are selected and illustrated in Figure 8 in order to interpret the EIS data. The physical significance of these models has been described in the literature [40-43]. In Figure 8, the symbol Q is used to signify the possibility of a non-ideal capacitance (CPE, constant phase element),

attributing to the distribution of relaxation times associated with heterogeneities at the surface of the electrode. Its impedance is defined as [41]:

$$Z_{CPE} = \frac{1}{Q(j\omega)^n} \qquad (2)$$

where Z_{CPE} represents the impedance of a CPE, Q is the modulus, ω and n are the angular frequency and the phase, respectively. The capacitor is considered ideal when n = 1, and non-ideal when 0.5 < n < 1.

The capacitance data obtained from EIS can be used to estimate the passive film thickness by using Eq. (3):

$$C = \frac{\varepsilon \varepsilon_0 A}{d} \qquad (3)$$

where ε is the dielectric constant (15.6), ε_0 is the vacuum permittivity (8.8542 × 10^{-12}F m^{-1}), A is the effective surface area of the sample, and d is the film thickness (m).

The EEC shown in Figure 8a is classically used to describe electro-chemical reaction at the electrode/electrolyte interface of a passive system, and an intact layer of passive film is considered [40]. Model B in Figure 8b is often regarded as the response from an inhomogeneous passive film, which consists of a porous outer layer and a compact inner layer [42,44]. Some literature considered that one of the two RQ elements represented the charge transfer process [43]. In Model C, the passive film is speculated to have a porous structure and to show non-ideal capacitive behavior. The Q1 and Q2 are associated with the oxide film and the electrical double layer, respectively. The point defect model (PDM) is taken into account in Model D and the migration in passive film is described by Warburg diffusion (W) [45]. The constant phase element Q_{diff} has also been used to represent the mass transfer process instead of the common element W [25]. Recently, Boissy et al. [42] explained the interest of combining a time constant with the diffusion-migration impedance associate d with the transport of vacancies through the oxide.

Experimental data were fitted with the Z-View Software. An iterative modeling process is used and the fit of a given model to the experimental data is determined from the chi-square (χ) value for the entire model and the percent error values for each circuit component. In this work the best fit was given by the model B in polluted phosphoric acid without abrasive and the model C in the polluted phosphoric acid solution with abrasive.
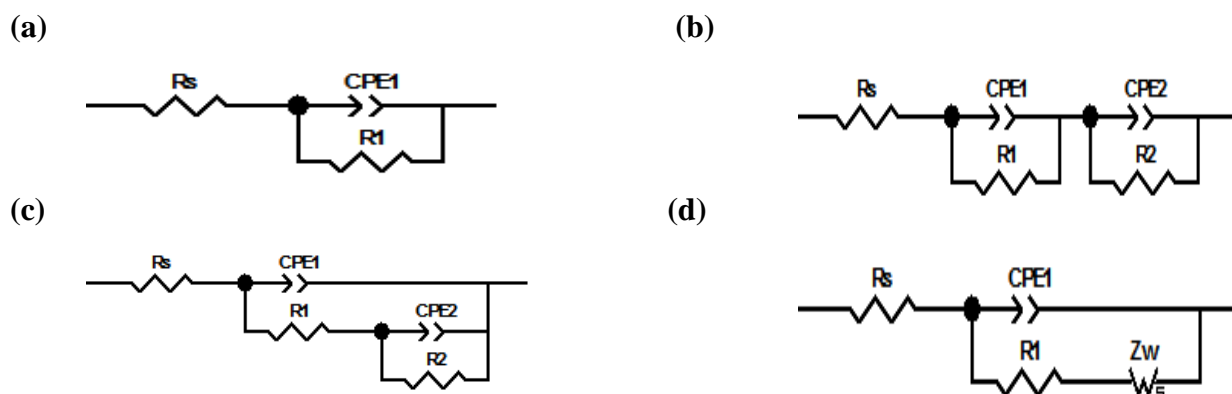

Figure 8: Four different models for interpretation of the impedance spectra on the passive metal surface: (a) Model A, (b) Model B, (c) Model C, (d) Model D.

In polluted phosphoric acid without abrasive the two R-CPE equivalent circuit [46] shown in Model B, the solution resistance R_s is connected in series with two time constants [(R$_1$CPE$_1$) (R$_2$CPE$_2$)]. In the first process (R$_1$//CPE$_1$), CPE$_1$ represents the double layer capacitance and R$_1$ is the corresponding charge-transfer resistance. In the second detected process (R$_2$//CPE$_2$), the values of CPE$_2$ and R$_2$ are associated with redox processes that can occur in the passive film. The parameter CPE$_2$ represents the capacitive behaviour of the passive film formed, coupled with a resistance R$_2$ due to the ionic paths through the passive film. Here, the constant phase element (CPE), which stands for a general diffusion related element, is used for the description of a frequency-independent phase shift between alternating potential and its current response.

In polluted phosphoric acid with abrasive R_s is the resistivity of the electrolyte, CPE_1 related to the capacitance of the outer porous oxide layer, R_1 is the resistance of the solution in the pores of the film, CPE_2 related to the capacitance of the inner protective oxide layer/electrolyte interface and R_2 is the charge transfer resistance occurring at the inner protective oxide layer/electrolyte interface. The use of a CPE is necessary to take into account the non-ideal capacitance behavior of the interfaces. The semiconductive behavior of oxide films associated to a charge carrier density lower than in metals leads to the development of a space charge layer capacity into the oxide layer, where almost all interfacial voltage is established [47,48]. The low value of the space charge layer capacity compared to the double layer capacity developed at the inner protective oxide layer/electrolyte interface make the double layer capacity not detectable. CPE_2 is thus related to the space charge layer capacity developed in the inner protective oxide layer at the inner oxide layer/electrolyte interface.

The electrical parameters obtained by adjusting the experimental data shown in Figure 7 are summarized in Table 4. According to the electrical parameters obtained, the resistance of the inner oxide layer (R_2) is larger than the values associated with the outer layer (R_1), which is consistent with the chosen physical model. These results indicate that the protection provided by the passive film is mainly due to the inner passive layer, known as the barrier layer, which is composed principally of chromium oxides. The resistance of the outer porous layer R_1 depends strongly on the existence of pores or defects, into which the electrolyte can penetrate and thus, R_1 provides a sensitive indication of the appearance of defects in the passive film.

It can be seen in Table 4, that R_1 decreases as added particles, which suggests that SiC particles favor the formation of a more porous film. On the other hand, the parameter R_2 associated with the inner oxide film is more sharply affected by particles. R_2 decreases with abrasive, which suggests a loss of the protective properties of the inner layer of the passive film. Simultaneously, the C_1 and C_2 increase with abrasive caused by decrease of the thickness of the layer of the film. Also, it can be observed that $C_1 > C_2$, which suggests that the inner layer of the passive film is thicker than the outer layer.

The estimated values of $d_T = d_1 + d_2$ show that the layers formed on Alloy 59 were typically on the order of nm in thickness and within the typical range for passive films formed on stainless steels (1-3 nm) [49].

Table 4: The fitted electrochemical parameters for EIS of austenitic stainless steel alloy 59 (UNS N-06059) in polluted phosphoric acid with and without abrasive.

	Rs (Ω cm²)	n_1	R_1 (Ω cm²)	C_1 (μF/cm²)	d_1 (nm)	n_2	R_2 (Ω cm²)	C_2 (μF/cm²)	d_2 (nm)	d_T (nm)	χ (10^{-3})
(a)	4.87	0.755	1733	53.80	0.26	0.945	217180	13.02	1.06	1.32	8.9
(b)	9.22	0.615	1356	31.11	0.44	0.930	65348	27.19	0.51	0.95	7.7

Note : (a) : Without abrasive particles (b) : With abrasive particles

3.5. Capacitance measurements (Mott-Schottky approach)

The electrochemical capacitance of the passive film/electrolyte interface was measured as a function of the applied potential to assess the semiconducting properties of the passive films formed on Alloy 59 in the contaminated H_3PO_4 solution. Since the space charge region developed in the passive film and the Helmholtz layer can be considered as two capacitors in series, the measured capacitance of the film/electrolyte interface can be written as (Equation 4) [50,52]:

$$\frac{1}{C} = \frac{1}{C_{SC}} + \frac{1}{C_H} \qquad (4)$$

where C_{SC} is the capacitance of the space charge layer and C_H is the capacitance of the Helmholtz layer. The validity of the Mott-Schottky (M–S) analysis is based on the assumption that the Helmholtz layer capacitance is so large than that the space charge layer capacitance. The total capacitance measured can be treated as the space charge layer capacitance and the potential drop caused by the applied potential occurs entirely within the space charge region [52]. Therefore, it should not be neglected, particularly in highly doped semiconductors, such as passive films [50,51]. In this case, the relationship between capacitance and the applied potential is given by the well-known Mott6Schottky equations (5,6) [53,54]:

$$\frac{1}{C^2} = \frac{1}{C_H^2} + \frac{2}{e \times N \times \varepsilon \times \varepsilon_0} \left(E - E_{FB} - \frac{KT}{e} \right) \qquad \text{n-type} \qquad (5)$$

$$\frac{1}{C^2} = \frac{1}{C_H^2} - \frac{2}{e \times N \times \varepsilon \times \varepsilon_0}\left(E - E_{FB} - \frac{KT}{e}\right) \qquad \text{p-type} \qquad (6)$$

where N charge carrier density (cm^{-3}), the donor density for n-type or the acceptor density for p-type semiconductors, e is the electron charge (1.6×10^{-19}C), ε_0 the vacuum permittivity (8.85×10^{-14}F cm^{-1}), ε the relative dielectric constant of the semiconductor, k Boltzmann's constant (1.38×10^{-23} J/K) and T absolute temperature, E is the applied electrode potential and E$_{FB}$ the flat band potential.

The data points on the $1/C^2_{SC}$ versus E plot can describe the semiconductive behavior of the depletion region.

Figure 10a and 10b display the Mott-Schottky curves for the passive films formed in the contaminated phosphoric acid solution with and without abrasive particles at the formation potential of 600 mV/SCE. Firstly, it should be noted that capacitance clearly decrease with added of particles, which is consistent with the results of the polarization curves and EIS measurements.
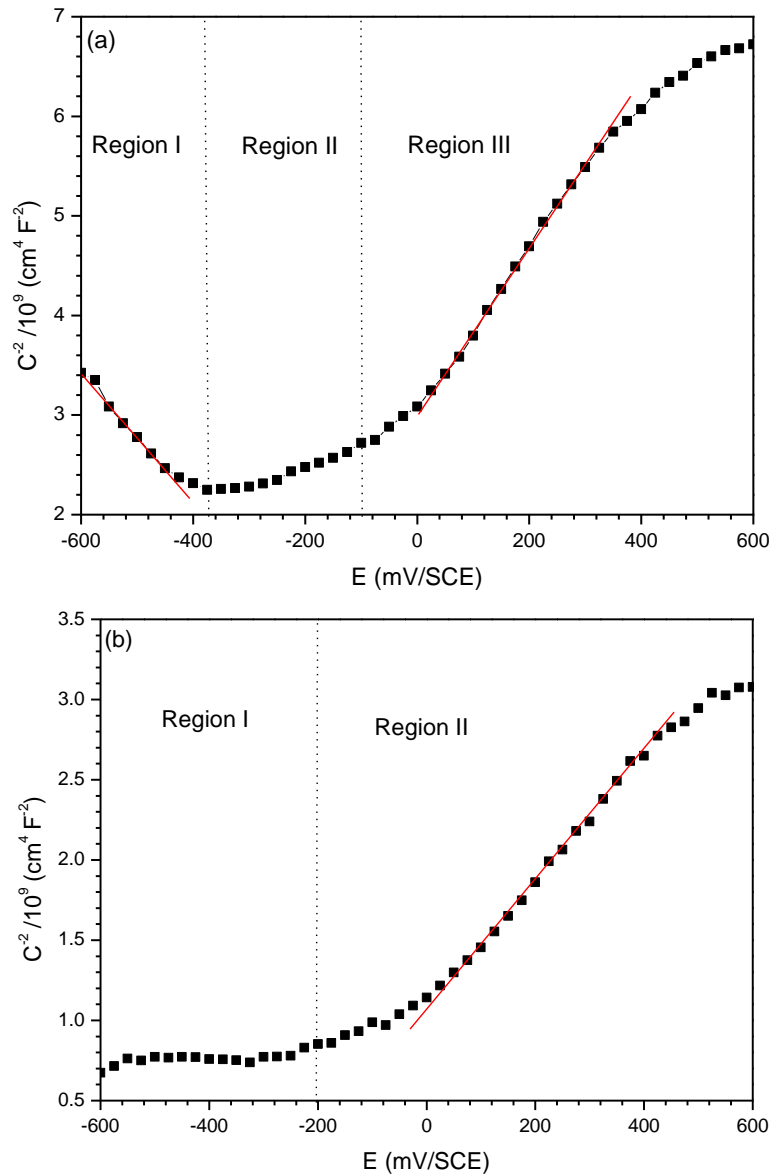

Figure 10: Mott-Schottky plots of passive films formed on Alloy 59 in the 40wt. % H$_3$PO$_4$contamined solution (a) without and (b) with the presence of abrasive particles.

The diagram obtained in the absence of abrasive particles (Figure 10a) show three regions in which two linear relationships between C^{-2} and E may be observed. In region I, the slope of the Mott-Schottky diagram is negative which is attributed to a p-type behaviour, probably due to the presence of Cr$_2$O$_3$, FeO and NiO on the

passive films [55]. In region II, the slope of Mott-Schottky plot is close to zero, whereas region III reveals positive slopes, indicating the n-type semiconducting behaviour of the passive films.

On the other hand, the Mott–Schottky diagram obtained in the presence of abrasive particles (Figure 10b), show two regions in which a linear relationship between C^{-2} and E can be observed. In region I, the slope of the Mott-Schottky diagrams is close to zero, whereas region II reveals positive slope, indicating the n-type semiconducting behaviour of the passive films.

However, passive films of nickel base alloys are considered to be highly doped semiconductors with an inner region essentially formed of Cr_2O_3 and an outer region mainly composed of hydroxides. Inside the potential region above E_{FB}, straight lines with negative slopes can be observed (Figure 10a), indicative that p-type semiconductor behavior of Cr_2O_3. It is similar to previous report for anodic passive films formed on iron, stainless steels and some alloys [56,57]. The C^{-2} vs. E curves also shows that there is a progressive change in the sign of the linear region slope at high potentials, going from positive to negative values in the case of the absence of abrasive particles. This phenomenon indicates a modification in the electronic properties of the passive film, from n-type to p-type semiconductivity, and is related to an increase in the conductivity of the film due to the solid state oxidation of Cr (III) to Cr (VI) [58,59]. On the contrary, inside the potential region below E_{FB}, the slope of the straight line is positive, so the capacitance measured corresponds to a n-type semiconductor with characteristic of hydroxides.

According to the following equation, the values of donor density N_D and acceptor density N_A can be determined from the slope of the experimental C^{-2} vs. E plots and the obtained values are summarized in Table 5.

$$N = \pm \frac{2}{m \times e \times \varepsilon \times \varepsilon_0} \qquad (7)$$

where m is the slope of the Mott-Schottky plot in the linear-region of interest, e is the electron charge, ε the relative dielectric constant of the semiconductor and ε_0 the vacuum permittivity.

Table 5: Evolution of the donors and acceptors densities with added particles calculated from Mott-Sckottky experiments.

Parameters	N_A (10^{21} cm^{-3})	N_D (10^{21} cm^{-3})
Without abrasive particles	1.42	1.09
With abrasive particles	-	2.24

The values of N_A and N_D for Alloy 59 are of the order of 10^{21} cm^{-3} in agreement with those reported for various austenitic stainless steels [60-62]. The donor density value slightly increases with the presence of the abrasive particles means that the passive film on Alloy 59 has higher electron density and lower impedance, as observed in the EIS measurements. All these statements confirm that the protective ability of the passive films formed on Alloy 59 decreases with abrasive particles. As a consequence, the aggressive ions, Cl^- and SO_4^{2-} have a great influence on the stability of the passive films which is consistent with the results obtained from the polarization and potentiostatic tests, and the images shown in Figure 5.

In addition, Tsuchiya [63] concluded that the passive film on Cr and Fe–Cr alloys can display both an n-type and a p-type behaviour in acidic media (case in the absence of abrasive particles), due to the double layer structure in the film and therefore, the n-type semiconducting behaviour of Alloy 59 can be mainly attributed to the chromium-enriched inner layer. Therefore, we conclude that in the case of the presence of abrasive particles, one layer structure in the film was rest the second can be removed by the effect of these abrasive particles.

Conclusion

Effect of abrasive particles on the electrochemical behaviour of passive film formed on Alloy 59 in 40wt. % H_3PO_4 contamined solution with 4wt. % H_2SO_4 and 0.42wt. % KCl was investigated using electrochemical measurements and microscopy analysis. Conclusions drawn from the study are as follows.

- The potentiodynamic polarization curves indicated that presence of SiC particles leads to increase on the corrosion rate of Alloy 59. This can be explained by that the presence of aggressive ions which is more aggressive with the presence of abrasive particles.

- The potentiostatic tests have shown that in the presence of abrasive particles, the current became higher at given potential of 600 mV/SCE indicating the equilibrium between the current dissolution of the active sites of the particles created by the abrasion and the current growth of passive layers
- The EIS results have showed that the action of abrasion causes accelerated corrosion of process leading to decreases the polarization resistance of the outer porous and inner oxide layer. This last, suggests that SiC particles favor the formation of a more porous film and a loss of the protective properties of the inner layer of the passive film. Capacitance values increased, simultaneously, with abrasive caused by decrease of the thickness of the layer of the film.
- The Mott-Schottky plots have shown both p-type and n-type semiconducting behaviours in the absence of abrasive particles where n-type in the presence of abrasive particles. Calculated acceptor/donor densities of Alloy 59 in polluted phosphoric acid revealed an increase of the donor densities with the presence of abrasive particles, which they are of the order of 10^{21} cm^{-3}. According to the obtained results, it can be concluded that the passive film formed on Alloy 59 stainless steel has a disordered structure and becomes more defective at added of particles.

References

1. Stachowiak G.B., Salasi M., Rickard W.D., Stachowiak G.W., *Corros. Sci.* 111 (2016) 690–702.
2. Arabnejad H., Shirazi S.A., McLaury B.S., Subramani H.J., Rhyne L.D., *Wear.* 332-333 (2015) 1098–1103.
3. Abu-eishah S.I., Abu-jabal N.M., *Chem. Eng. J.* 81 (2001) 231-250.
4. Santos M.B., Labiapari W.S., Ardila M.A.N., Silva W.M., De Mello J.D.B., *Wear.* 332-333 (2015) 1206-1214.
5. Guenbour A., Faucheu J., Ben Bachir A., Dabosi F., Bui N., *Brit. Corros. J.* 23 (1988) 234-238.
6. Calderón J.A., Henao J.E., Gómez M.A., *Electrochim. Acta.* 124 (2014) 190-198.
7. Escrivà-Cerdán C., Blasco-Tamarit E., García-García D.M., García-Antón J., Guenbour A., *Corros. Sci.* 56 (2012) 114-122.
8. Sánchez-Tovar R., Montañés M.T., García-Antón J., Guenbour A., *Mater. Chem. Phys.* 133 (2012) 289-298.
9. Oñoro J., Int. J. Pres. Ves. Pip. 86 (2009) 656-660.
10. Freire L., Carmezim, Ferreira M.G.S., Montemor M.F., *Electrochim. Acta.* 56 (2011) 5280-5289.
11. Jakupi P., Zagidulin D., Noël J.J., Shoesmith D.W., *Electrochim. Acta.* 56 (2011) 6251-6259.
12. Gray J.J., Orme C.A., *Electrochim. Acta.* 52 (2007) 2370-2375.
13. Burstein G.T., Daymond B.T., *Corros. Sci.* 51 (2009) 2249-2252.
14. Newman R.C., Sieradzki K., Isaacs H.S., *Metall. Trans. A* 13 (1982) 2015-2026.
15. Mudgal D., Singh S., Prakash S., *J. Mater. Eng. Perform.* 24 (2015) 1-15.
16. Bellaouchou A., Kabkab B., Guenbour A., Ben Bachir A., *Prog. Org. Coatings.* 41 (2001) 121-127.
17. Saoudi N., Bellaouchou A., Guenbour A., Ben Bachir A., Essassi E.M., El Achouri M., *Bull. Mater. Sci.* 33 (2010) 313-318.
18. Lgamri A., El Makarim H.A., Guenbour A., Ben Bachir A., Aries L., El Hajjaji S., *Prog. Org. Coatings.* 48 (2003) 63-70.
19. El Hajjaji S., Lgamri A., Aziane D., Guenbour A., Essassi E.M., Akssira M., Ben Bachir A., *Prog. Org. Coatings.* 38 (2000) 207-212
20. Guenbour A., Hajji M.A., Jallouli E.M., Ben Bachir A., *Appl. Surf. Sci.* 253 (2006) 2362-2366.
21. Ibáñez-Ferrándiz M., Blasco-Tamarit E., García-García D.M., Garcia- Antona J. , Guenbour A. , Bakour S. , *ECS Trans.* 25 (2010) 49-61.
22. Olsson C.O.A, Landolt D., *Electrochim. Acta.* 48 (2003) 1093-1104.
23. Hayes J.R., Gray J.J., Szmodis A.W., Orme C.A., *Corros.* 62 (2006) 491-500.
24. López D., Alonso Falleiros N., Paulo Tschiptschin A., *Tribol. Int.* 44 (2011) 610-616.
25. Luo H., Gao S., Dong C., Li X., *Electrochim. Acta.* 135 (2014) 412-419.
26. Trzaskoma P. P., McCafferty E., Crowe C. R., *J. Elecrochem. Soc.* 130 (1983) 1804-1809
27. Toptan F., Alves A.C., Kerti I., Ariza E., Rocha L.A., *Wear.* 306 (2013) 27-35.
28. Stack M.M., Rodling J., Mathew M.T., Jawan H., Huang W., Park G., Hodge C., *Wear.* 269 (2010) 376-382.
29. Escriv-Cerdán C., Blasco-Tamarit E., García-García D.M., García-Antón J., Guenbour A., *Electrochim. Acta.* 80 (2012) 248-256.

30. Benea L., Wenger F., Ponthiaux P., Celis J.P., *Wear*. 266 (2009) 398-405.
31. Lakatos-Varsányi M., Falkenberg F., Olefjord I., *Electrochim. Acta*. 43 (1998) 187-197.
32. Sadiq K., Black R.A., Stack M.M., *Wear*. 316 (2014) 58-69.
33. Qiao Y.X., Zheng Y.G., Ke W., Okafor P.C., *Corros. Sci*. 51 (2009) 979-986.
34. Lee J.B., *Mater. Chem.Phys*. 99 (2006) 224-234.
35. Fernández-Domene R.M., Blasco-Tamarit E., García-García D.M., García-Antón J., *Corros. Sci*. 52 (2010) 3453-3464.
36. Galvele J.R., Torresi R.M., Carranza R.M., *Corros. Sci*. 31 (1990) 563-571.
37. Szklarska-Smialowska Z., *Corros. Sci*. 41 (1999)1743-1767.
38. El-Taib Heakal F., Ghoneim A., Fekry M., *J. Appl. Electrochem*. 37 (2007) 405-413.
39. Ismail Kh.M., *Electrochim. Acta*. 52 (2007) 781-819.
40. Kocijan A., Merl D.K., Jenko M., *Corros. Sci*. 53 (2011) 776-783.
41. Mohammadi F., Nickchi T., Attar M., Alfantazi A., *Electrochim. Acta*. 56 (2011) 8727-8733.
42. Boissy C., Ter-Ovanessian B., Mary N., Normand B., *Electrochim. Acta*. 174 (2015) 430-437.
43. Ge H.-H., Zhou G.-D., Wu W.-Q., *Appl. Surf. Sci*. 211 (2003) 321-334.
44. Chen T., John H., Xu J., Lu Q., Hawk J., Liu X., *Corros. Sci*. 77 (2013) 230-245.
45. Fernández-Domene R.M., Blasco-Tamarit E., García-García D.M., García-Antón J., *Electrochim. Acta*. 95 (2013) 1-11.
46. Andrade C., Keddam M., Nóvoa X. R., Pérez M. C., Angle C. M. R., Takenouti H., *Electrochim. Acta*. 46 (2001) 3905-3912.
47. Lavigne O., Alemany-Dumont C., Normand B., Berger M.H., Duhamel C., Delichere P., *Corros. Sci*. 53 (2011) 2087-2096.
48. Lavigne O., Takeda Y., Shoji T., Sakaguchi K., *Corros. Sci*. 53 (2011) 1079-1085.
49. Olsson C.-O.A., Landolt D., *Electrochim. Acta*. 48 (2003) 1093-1104.
50. Hakiki N.B., Boudin S., Rondot B., Da Cunha Belo M., *Corros. Sci*. 37 (1995) 1809-1822.
51. Uosaki K., Kita H., *J. Electrochem. Soc*. 130 (1983) 895-897.
52. Hakiki N.E., Ferreira M.G.S., *J. Electrochem. Soc*. 145 (1998) 3821-3829.
53. Gomes W.P., Vanmaekelbergh D., *Electrochim. Acta*. 41 (1996) 967-973.
54. Macdonald D.D., *J. Electrochem. Soc*. 153 (2006) B213-B224.
55. Cheng X., Li X., DU C., *Chin. Sci. Bull.* 54 (2009) 2239-2246.
56. Amri J., Souier T., Malki B., Baroux B., *Corros. Sci*. 50 (2008) 431-435.
57. Sunseri C., Piazza S., Di Quarto F., Chimica I., Palermo U., Scienze V., *J. Electrochem. Soc*. 137 (1990) 2411-2417.
58. Bojinov M., Fabricius G., Laitinen T., Saario T., Sundholm G., *Electrochim. Acta*. 44 (1998) 247-261.
59. Zhang H., Zhao Y., Jiang Z., *Mater. Lett*. 59 (2005) 3370-3374.
60. Metikoš-Huković M., Babić R., Grubač Z., Petrović Ž., Lajçi N., *Corros. Sci*. 53 (2011) 2176-2183.
61. Ferreira M.G.S., Da Cunha Belo M., Hakiki N.E., Goodlet G., Montemor M.F., Simõesa A.M.P., *J. Braz. Chem. Soc*. 13 (2002) 433-440.
62. Carmezim M.J., Simões A.M., Montemor M.F., Da Cunha Belo M., *Corros. Sci*. 47 (2005) 581-591.
63. Tsuchiya H., Fujimoto S., Chihara O., Shibata T., *Electrochim. Acta*. 47 (2002) 4357-4366.

(2017) ; http://www.jmaterenvironsci.com